Critical Analysis of an FeP Empirical Potential Employed to Study the Fracture of Metallic Glasses

Yezeng He,[1,2] Peng Yi,[2,5] and Michael L. Falk[2,3,4,5,*]
[1]School of Materials Science and Engineering, China University of Mining and Technology, Xuzhou 221116, People's Republic of China
[2]Materials Science and Engineering, Johns Hopkins University, Baltimore, Maryland 21218, USA
[3]Mechanical Engineering, Johns Hopkins University, Baltimore, Maryland 21218, USA
[4]Physics and Astronomy, Johns Hopkins University, Baltimore, Maryland 21218, USA
[5]Hopkins Extreme Materials Institute, Johns Hopkins University, Baltimore, Maryland 21218, USA

(Received 23 September 2018; published 24 January 2019)

An empirical potential that has been widely used to perform molecular dynamics studies on the fracture behavior of FeP metallic glasses is shown to exhibit spinodal decomposition in the composition range commonly studied. The phosphorous segregation induces a transition from ductility to brittleness. During brittle fracture the atomically sharp crack tip propagates along a percolating path with higher P concentration. This embrittlement is observed to occur over a wide range of chemical compositions, and toughness decreases linearly with the degree of compositional segregation over the entire regime studied. Stable glass forming alloys that can be quenched at low quench rates do not, as a rule, exhibit such thermodynamically unstable behavior near to or above their glass transition temperatures. Hence, the microstructures exhibited in these simulations are unlikely to reflect the actual microstructures or fracture behaviors of the glassy alloys they seek to elucidate.

DOI: 10.1103/PhysRevLett.122.035501

Introduction.—Metallic glasses (MGs) have drawn considerable attention as promising structural materials due to their unique combination of properties such as high strength, extreme hardness, and superior corrosion resistance [1–5]. However, the limited ductility of MGs restricts their use in various structural, engineering, and functional applications [6]. Considerable scientific efforts have been made to unravel the physics of deformation and fracture in these materials in order to guide efforts to increase their toughness. Even so, controversies remain about the failure and fracture mechanisms of MGs [7,8].

Recent theoretical and experimental studies have demonstrated that many factors will influence the fracture behavior of MGs. For instance, Lewandowski *et al.* [9] compared properties of numerous MGs and reported a critical Poisson's ratio exists around 0.31–0.32 below which the MGs are observed to be brittle. However, no fundamental explanation for this empirically observed relation currently exists. Murali *et al.* [10] has investigated the susceptibility of $Zr_{41.2}Ti_{13.75}Cu_{12.5}Ni_{10}Be_{22.5}$ MGs to embrittlement upon annealing and found that the toughness declines by up to 90%. Rycroft and Bouchbinder [11] attributed the annealing-induced embrittlement transition to the existence of an elastoplastic instability that induces cavitation ahead of the crack tip for sufficiently relaxed glasses. This is supported by recent experimental studies that link the fictive temperature, sometimes also referred to as the effective temperature, to a brittle-to-ductile transition in these materials that is highly sensitive to loading rate [12]. This reinforces the relevance of a number of simulation studies of cavitation in MGs that have been undertaken with the stated aim of more fully understanding the fracture process zone [13–15]. Moreover, the residual stress and alloy composition may also play important roles in the fracture behavior of MGs [16–18]. Despite intense investigation, theoretically predicting the fracture behavior of MGs remains a challenge.

In recent years, molecular dynamics (MD) simulations have been used to directly examine brittle and ductile fracture behavior in MG materials [19–21]. A number of embedded atom method (EAM) interatomic potentials have been used for these studies including a common model for CuZr [22] and an FeP potential that was originally created to mimic the behavior of P impurities in steels [23]. Notably the FeP potential appears to be one of the few models of an amorphous alloy that results in brittle behavior on the sub-μm scale, making it an attractive system for examining a range of mechanical response regimes using atomistic simulations. However, it is important to note that this potential was not designed to mimic realistic phase behavior in either the crystalline or liquid phases. The main motivation for the development of this potential was described upon its publication as such [23], "For molecular dynamics purposes in studying reactor steels, the interesting region is that of small concentrations ($\sim 10^{-3}$) of P in Fe, in particular, the behaviour of point

defects in lattices." The authors of this potential further note that, "Pure P is covalently bonded and cannot be described by this type of potential. We therefore do not attempt to fit properties of pure phosphorus, or phosphorus-rich compounds, concentrating instead on point defects in α-iron…" Therefore, we ask the questions, "What is the underlying phase behavior of this potential?" and "How do the thermodynamic driving forces arising from this potential influence the fracture behavior exhibited by this model?" Our investigation provides evidence that this particular FeP potential exhibits spinodal decomposition, and it is the resulting compositional segregation, which depends sensitively on the thermal processing history, that determines the fracture behavior of the simulated MG model.

Methods.—In this study, MD simulations were used to investigate the fracture behavior using the EAM potential parametrized by Ackland *et al.* [23] that has been previously applied to model FeP MG fracture [20,21]. All the simulations were conducted using the LAMMPS software package [24]. The Nosé-Hoover thermostat and Parinello-Rahman barostat are used to control the temperature and pressure, respectively. The velocity-verlet algorithm is used to integrate the equations of motion with a time step of 2 fs. Periodic boundary conditions were applied in all directions. Two different ways were used to prepare a system, and we will refer to these as melted and quenched (MQ) and annealed (A). For MQ systems, 162 000 atoms were initially arranged as a disordered body-centered cubic (BCC) structure with P atomic percentage of 15%, 20%, or 25%. The temperature of this system was raised gradually to 2000 K and equilibrated for 20 ns, followed by a cooling process to 1 K at a quench rate of 1 K/ps and a subsequent relaxation process for 2 ns at 1 K. Alternatively, suddenly quenched and annealed systems were prepared as follows. Initially consisting of 162 000 Fe atoms, the systems were first processed as the melted-and-quenched simulation as explained above. Then a fraction of Fe atoms (15%, 20%, or 25%) were randomly substituted with P atoms. Subsequently, we anneal these systems for 1 ns at 1, 500, 600, 700, and 800 K. We designate these systems A1, A500, A600, A700, and A800, respectively. For the above simulations, the *NPT* ensemble was employed and the pressure was maintained at zero. The resulting samples have dimensions of approximately 530 Å × 265 Å × 15 Å. To study the fracture phenomena, we create a fracture specimen from each sample by introducing a sharp crack of length 100 Å through removing atoms in the middle of the sample. Finally, the samples were stretched at a strain rate of 0.05/ns along the direction perpendicular to the crack face. During the tensile process, the temperature was maintained at 1 K to eliminate the thermal effects using the Nosé-Hoover thermostat and the boundaries perpendicular to the crack face were held fixed to eliminate the Poisson effects.

Results and discussion.—To begin, we consider the $Fe_{85}P_{15}$ system as an example to illustrate the structure of the system obtained via the traditional melting-and-quenching process. In Fig. 1(a), compared to the initial configuration, the final configuration of a MQ sample shows P aggregation, in which the P atoms aggregate into a continuous fractal structure. To verify that this system is thermodynamically driven toward P aggregation, we consider the thermodynamic relation

$$\Delta G_{\mathrm{mix}} = -T\Delta S_{\mathrm{mix}} + \Delta H_{\mathrm{mix}}, \tag{1}$$

where ΔG_{mix}, ΔS_{mix}, and ΔH_{mix} are the change of mixing Gibbs free energy, entropy, and enthalpy, respectively. The mixing entropy can be calculated using an ideal solution approximation, which is valid in the dilute limit,

$$\Delta S_{\mathrm{mix}} = -R(x_{\mathrm{Fe}} \ln x_{\mathrm{Fe}} + x_P \ln x_P), \tag{2}$$

where x_{Fe} and x_P are the atomic concentrations of Fe and P atoms, respectively. The mixing enthalpy change can be expressed as

$$\Delta H_{\mathrm{mix}} = H_{\mathrm{mix}} - H_{\mathrm{Fe}} x_{\mathrm{Fe}} - H_P x_P, \tag{3}$$

where H_{mix}, H_{Fe}, and H_P are the enthalpy of mixed phase, pure Fe, and pure P, respectively. Then, the second derivative of ΔG_{mix} with respect to x_P gives

$$\frac{d^2\Delta G_{\mathrm{mix}}}{dx_P^2} = RT\left(\frac{1}{x_P} + \frac{1}{1-x_P}\right) + \frac{d^2 H_{\mathrm{mix}}}{dx_P^2}. \tag{4}$$

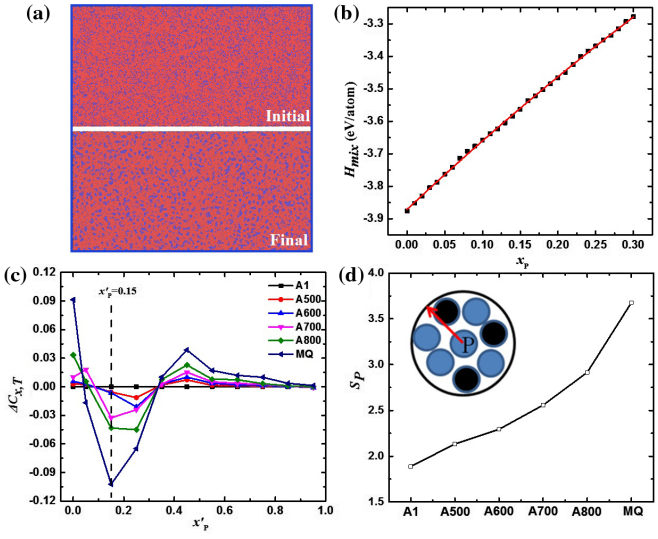

FIG. 1. (a) Initial and final structures of $Fe_{85}P_{15}$ during the traditional melting-and-quenching process. Blue: P atoms; red: Fe atoms. (b) Change of H_{mix} versus x_p. (c) Fluctuation of P concentrations within 5 Å voxels relative to the A1 system. (d) P segregation S_P defined as the average number of P near neighbors of each P atom, as a function of system preparation. A1 denotes annealing at 1 K for 1 ns starting from a glass with randomly located P atoms. A500 denotes the same process at 500 K, etc. MQ denotes a system that was quenched from the $Fe_{85}P_{15}$ melt.

We calculated H_{mix} through the MD simulations using the FeP potential. Figure 1(b) shows the fitting of H_{mix} as a function of x_P to a second order polynomial. Then, by equating the second derivative of ΔG_{mix} in Eq. (4) to zero, the spinodal temperature for mixture $Fe_{85}P_{15}$ can be found to be 1985 K, which is far above the glass transition temperature of about 950 K [25,26]. This thermodynamic analysis would predict spinodal decomposition at the glass transition temperature, which is consistent with our observations of the P aggregation in the simulations.

To further examine that compositional segregation plays a strong role in the microstructure, we have created a series of suddenly quenched systems annealed at different temperatures, A1-A800, as described above. To analyze the phase separation, the $Fe_{85}P_{15}$ system was divided into cubic voxels with side length 5 Å, and the P concentrations over these grids were collected. Figure 1(c) shows the difference between the A1 system and other systems, which indicates the degree of segregation as the composition systematically diverges from the mean composition to enhance higher and lower composition regions, the distribution eventually becoming bimodal. Another measure we used to characterize the phase separation is the degree of compositional segregation S_P. We define S_P as the average number of P atoms within a near-neighbor distance of any P atom as the inset shows in Fig. 1(d). The near neighbor distance 3.475 Å was chosen from the first trough in the radial distribution function of pure P in a BCC structure modeled with this potential. Although S_P increases with the annealing temperature, it is always smaller than that found in the MQ system.

During the loading process, the system undergoes failure by the propagation of a crack, consistent with previously reported results [20,21]. Figure 2(a) shows the related stress-strain curves. It can be found that the $Fe_{85}P_{15}$ MGs experience a gradual transition from ductility to brittleness with the increase of annealing temperature. For instance, the A1 sample that failed at ~6.5 GPa exhibited larger plastic strain, 4.3%, as compared to near zero plastic strain in the A800 sample before fracture. During the fracture process, the stress decreases as the strain increases. Every dramatic drop in stress is correlated with the propagation of the crack and every plateau is correlated with a period of plastic deformation in the crack tip process zone [27]. We note that the strain at which the systems completely fracture also increases with the annealing temperature, further indicating a decrease in ductility. We can compute the toughness of these systems in order to quantify their ability to resist fracture [28]. The toughness is defined as the area under the stress-strain curve. While the toughness measured in this manner is not a material property, it is a reasonable measure of the fracture resistance of the material under the specific load conditions given the geometry of the fracture test applied. Our results, given in Fig. 2(b), show that the toughness monotonically decreases with the annealing temperature.

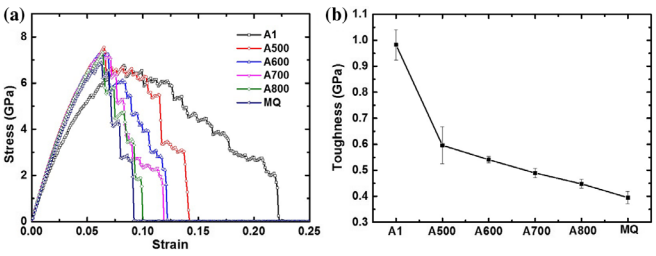

FIG. 2. Stress-strain curves (a) and related toughness (b) of $Fe_{85}P_{15}$ obtained at different annealing temperatures.

Generally speaking, composition plays a key role in determining the microstructure and properties of materials. We can now directly correlate S_P in this model with the toughness of systems with different compositions that have been exposed to different annealing temperatures. As shown in Fig. 3, a similar trend has been found in the $Fe_{80}P_{20}$ and $Fe_{75}P_{25}$ systems as in the $Fe_{85}P_{15}$ system. Moreover, we can expect that an increase in the P concentration will result in a higher S_P at the same annealing temperature. In addition, the system containing more P atoms always has a lower toughness as shown in Fig. 3(b).

As mentioned above, the annealing process and the alloy composition affect both the microstructure and the resulting toughness within this model of FeP MGs. Next we check whether there exists any correlation between the S_P and the toughness. Figure 3(c) shows the change of toughness as a function of S_P for all the systems investigated above. It is found that the toughness decreases monotonically with S_P except for the highly unstable A1 samples. For the other well-annealed systems, the toughness decreases linearly with S_P independent of chemical composition, as shown in Fig. 3(d).

The results above clearly show that changing annealing temperature induces changes in the glass microstructure of this model system arising from phase separation, and this

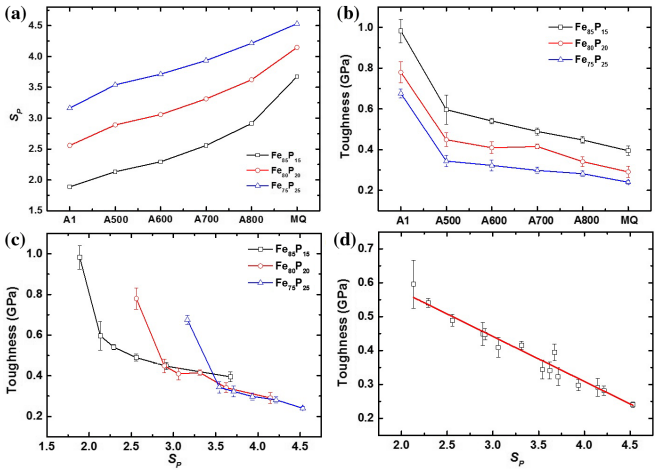

FIG. 3. Effect of annealing temperature on S_P (a) and the toughness (b) of different alloy systems. (c) Toughness as a function of S_P. (d) Toughness versus S_P of all except the A1 systems.

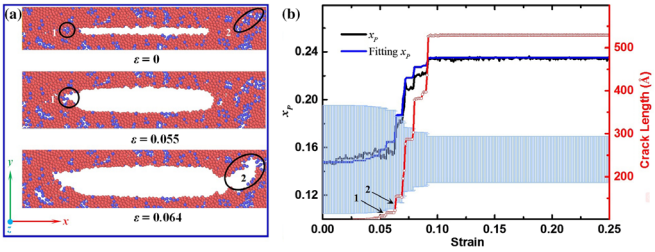

FIG. 4. Structural evolution of crack during the uniaxial tensile loading of MQ-$Fe_{85}P_{15}$. (a) The crack, initially 100 Å in length (x direction) and 5 Å in width (y direction) at several applied strains along the y direction. Numbered circles show significant crack advancement events also denoted in the graph to the right. (b) Plot showing the change of crack length (red circles) and the P atom concentration at crack surface (black line) x_P during mechanical loading. Plot additionally shows a fitted expression for the expected mean value of x_P (blue) assuming that the crack incorporates P atoms into the growing crack surface at a probability $p = 0.255$, despite the fact that the likelihood of a randomly chosen atom being a P atoms is 0.15. Error bars centered on $x_P = 0.15$ show the range of concentration within one standard deviation of the expected mean value for the P concentration on the crack surface if the crack surface were incorporating atoms irrespective of species.

compositional segregation correlates strongly with embrittlement. Previous experimental evidence has shown that processing effects such as cooling rate and processing environment also influence the fracture behavior of MGs [29]. Therefore, the observed phase separation may not be the only or even the primary cause of embrittlement arising from changing processing condition. To explore the fracture mechanism in more detail, Fig. 4(a) shows the structural evolution of crack during the tensile process. It can be found that the sharp crack tip propagates towards P-rich regions which appear to be amenable to nanoscale cavitation, such that every advance of the crack begins with the expansion of a cavity.

The initial crack is introduced by creating a rectangular cavity of length 100 Å (along the x direction) and width 5 Å (along the y direction) from an annealed sample, as shown in Fig. 4(a). The crack extends infinitely along the z direction due to periodic boundary conditions. A uniaxial tensile strain is applied in the y direction. To determine the length of the crack upon loading, the system is divided into slices normal to the x direction with a slice width of $\rho_N^{-1/3}$, 2.35 Å. For each slice, the atoms are sorted based on their y coordinates. If the difference in the y coordinate between any two neighboring atoms is greater than the near-neighbor distance of P atoms, 3.475 Å, this slice is considered to have been fractured. The two atoms so identified are considered to be the outermost atoms on the fracture surface. These two atoms, and all the atoms in the same slice that are within 2.35 Å in y coordinate from either of these two atoms, are counted as surface atoms of the fracture. Compositional analysis was subsequently performed over the surface atoms for all slices. As shown in Fig. 4(b), the P concentration increases steadily with the crack propagation, exceeding the average concentration of 15% even at the beginning of fracture and rising to nearly 23.5%. This indicates that the atomically sharp crack tip propagates along a surface with higher P concentration. We can fit the change in concentration along the crack path with a one parameter curve that assumes that the probability for the crack tip to incorporate a P atom rather than an Fe atom is 0.255, 170% of the expected probability if the atoms were chosen randomly. We further show, as error bars, the region of concentration within one standard deviation of the expected mean concentration in a scenario where the crack propagates randomly. Clearly the concentration along the crack tip is far outside this range, reaching as high as 0.235. The likelihood of achieving such a P-rich crack surface by chance can be found by calculating the cumulative binomial distribution, and is a mere 2 in one million. This provides strong evidence that the previously described compositional segregation is strongly influencing the fracture behavior of this FeP MG model system.

According to previous studies, MGs containing two glassy phases have remarkable plasticity [30–32]. However, we come to completely opposite conclusions in this work regarding the system at hand. The reason for this puzzling behavior is that the P-rich phase is extremely brittle while the Fe-rich phase is more ductile. Clusters consisting of P atoms have a strong propensity for nanoscale cavitation in the region ahead of the crack tip. This along with the strong spinodal decomposition we observe explains why the atomically sharp crack tip propagates along a fracture plane with higher P concentrations as shown in Fig. 4(b).

Conclusion.—In this work, we have investigated the fracture behavior of a particular interatomic potential that has been extensively used to model the fracture behavior of FeP MGs using MD simulations. Our results clearly show that the system is unstable to spinodal decomposition, and due to this fact changing the annealing temperature results in drastically different degrees of compositional segregation. This compositional segregation is the dominant factor determining the resulting toughness of the model MGs. For well-annealed systems, the toughness decreases linearly with the degree of compositional segregation independent of chemical composition. As a result of this investigation we believe that this FeP EAM model is not a realistic system for the investigation of fracture in MG materials. The development of more realistic force fields that exhibit a range of ductility and that do not suffer from such a strong instability to spinodal decomposition would be an excellent goal for future work.

These observations also have significant implications for interpreting prior work performed using this potential model to study fracture. While we have no doubt that the brittleness in this model system arises for the reasons explained in Ref. [20], it is highly doubtful that real FeP

glasses, or any experimentally realized MG system with even marginal glass-forming ability, exists in such an extreme state of thermodynamic instability. One must then question whether the notch sensitivity experimentally measured in the NiP glass samples studied in Ref. [21] could be in any way adequately described by this model system. At the very least, if the notch sensitivity observed in NiP MG materials does arise from nanoscale cavitation, further study needs to be undertaken to understand the structural origin of this phenomenon. If it does arise from compositional segregation on the nanoscale, the thermophysical origin of this segregation would be a fascinating topic for future study. One possibility could be that in real marginal glass formers much more modest thermodynamic driving forces acting over substantially longer times lead to nanoscale compositional segregation not so different from that evident in this dramatically unstable computer model quenched at enormous rates.

M. L. F. acknowledges support by NSF under Grant No. 1408685/1409560. We also acknowledge the prior work and comments of Prof. Pengfei Guan of the Beijing Computational Sciences Research Center who helped inspire this work and who provided insightful comments on the manuscript, and Prof. Yunfeng Shi whose prior work inspired this investigation.

*Corresponding author.
mfalk@jhu.edu

[1] M. Telford, The case for bulk metallic glass, Mater. Today **7**, 36 (2004).
[2] J. Schroers and W. L. Johnson, Ductile Bulk Metallic Glass, Phys. Rev. Lett. **93**, 255506 (2004).
[3] C. A. Schuh, T. C. Hufnagel, and U. Ramamurty, Mechanical behavior of amorphous alloys, Acta Mater. **55**, 4067 (2007).
[4] M. Chen, A. Inoue, W. Zhang, and T. Sakurai, Extraordinary Plasticity of Ductile Bulk Metallic Glasses, Phys. Rev. Lett. **96**, 245502 (2006).
[5] T. C. Hufnagel, C. A Schuh, and M. L. Falk, Deformation of metallic glasses: Recent developments in theory, simulation, and experiments, Acta Mater. **109**, 375 (2016).
[6] J. Das, M. B. Tang, K. B. Kim, R. Theissmann, F. Baier, W. H. Wang, and J. Eckert, Deformation of Metallic Glasses: Recent Developments in Theory, Simulations, and Experiments, Phys. Rev. Lett. **94**, 205501 (2005).
[7] X. K. Xi, D. Q. Zhao, M. X. Pan, W. H. Wang, Y. Wu, and J. J. Lewandowski, "Work-Hardenable" Ductile Bulk Metallic Glass, Phys. Rev. Lett. **94**, 125510 (2005).
[8] G. Wang, D. Q. Zhao, H. Y. Bai, M. X. Pan, A. L. Xia, B. S. Han, X. K. Xi, Y. Wu, and W. H. Wang, Fracture of Brittle Metallic Glasses: Brittleness or Plasticity, Phys. Rev. Lett. **98**, 235501 (2007).
[9] J. J. Lewandowski, W. H. Wang, and A. L. Greer, Intrinsic plasticity or brittleness of metallic glasses, Philos. Mag. Lett. **85**, 77 (2005).
[10] P. Murali and U. Ramamurty, Embrittlement of a bulk metallic glass due to sub-Tg annealing, Acta Mater. **53**, 1467 (2005).
[11] C. H. Rycroft and E. Bouchbinder, Fracture Toughness of Metallic Glasses: Annealing-Induced Embrittlement, Phys. Rev. Lett. **109**, 194301 (2012).
[12] J. Ketkaew, W. Chen, H. Wang, A. Datye, M. Fan, G. Pereira, U. D. Schwarz, Z. Liu, R. Yamada, W. Dmowski, M. D. Shattuck, C. S. O'Hern, T. Egami, E. Bouchbinder, and J. Schroers, Mechanical glass transition revealed by the fracture toughness of metallic glasses, Nat. Commun. **9**, 3271 (2018).
[13] P. Guan, S. Lu, M. J. B. Spector, P. K. Valavala, and M. L. Falk, Cavitation in Amorphous Solids, Phys. Rev. Lett. **110**, 185502 (2013).
[14] Q. An, K. Samwer, M. D. Demetriou, M. C. Floyd, D. O. Duggins, W. L. Johnson, and W. A. Goddard, How the toughness in metallic glasses depends on topological and chemical heterogeneity, Proc. Natl. Acad. Sci. U.S.A. **113**, 7053 (2016).
[15] E. Bouchbinder and J. S. Langer, Nonequilibrium thermodynamics of driven amorphous materials. III. Shear-transformation-zone plasticity, Phys. Rev. E **80**, 031133 (2009).
[16] Y. Zhang, W. H. Wang, and A. L. Greer, Making metallic glasses plastic by control of residual stress, Nat. Mater. **5**, 857 (2006).
[17] T. Mukai, T. G. Nieh, Y. Kawamura, A. Inoue, and K. Higashi, Effect of strain rate on compressive behavior of a Pd40Ni40P20 bulk metallic glass, Intermetallics **10**, 1071 (2002).
[18] M. L. Lee, Y. Li, and C. A. Schuh, Effect of a controlled volume fraction of dendritic phases on tensile and compressive ductility in La-based metallic glass matrix composites, Acta Mater. **52**, 4121 (2004).
[19] M. L. Falk, Molecular-dynamics study of ductile and brittle fracture in model noncrystalline solids, Phys. Rev. B **60**, 7062 (1999).
[20] P. Murali, T. F. Guo, Y. W. Zhang, R. Narasimhan, Y. Li, and H. J. Gao, Atomic Scale Fluctuations Govern Brittle Fracture and Cavitation Behavior in Metallic Glasses, Phys. Rev. Lett. **107**, 215501 (2011).
[21] X. W. Gu, M. Jafary-Zadeh, D. Z. Chen, Z. Wu, Y. W. Zhang, D. J. Srolovitz, and J. R. Greer, Mechanisms of failure in nanoscale metallic glass, Nano Lett. **14**, 5858 (2014).
[22] Y. Q. Cheng and E. Ma, Atomic-level structure and structure–property relationship in metallic glasses, Prog. Mater. Sci. **56**, 379 (2011).
[23] G. Ackland, M. Mendelev, D. Srolovitz, S. Han, and A. Barashev, Development of an interatomic potential for phosphorus impurities in a-iron, J. Phys. Condens. Matter **16**, S2629 (2004).
[24] S. Plimpton, Fast parallel algorithms for short-range molecular dynamics, J. Comput. Phys. **117**, 1 (1995).
[25] N. Rena, B. Shang, P. Guan, and L. Hu, General structural and dynamic characteristics beneficial to glass-forming ability of Fe-based glass-forming liquids, J. Non-Cryst. Solids **481**, 116 (2018).
[26] X. J. Liu, S. D. Wang, H. Wang, Y. Wu, C. T. Liu, M. Li, and Z. P. Lu, Local structural mechanism for frozen-in dynamics in metallic glasses, Phys. Rev. B **97**, 134107 (2018).

[27] C. A. Schuh and T. G. Nieh, A nanoindentation study of serrated flow in bulk metallic glasses, Acta Mater. **51**, 87 (2003).

[28] D. C. Hofmann, J. Y. Suh, A. Wiest, G. Duan, M. L. Lind, M. D. Demetriou, and W. L. Johnson, Designing metallic glass matrix composites with high toughness and tensile ductility, Nature (London) **451**, 1085 (2008).

[29] W. Chen, H. Zhou, Z. Liu, J. Ketkaew, N. Li, J. Yurko, N. Hutchinson, H. Gao, and J. Schroers, Processing effects on fracture toughness of metallic glasses, Scr. Mater. **130**, 152 (2017).

[30] J. W. Qiao, A. C. Sun, E. W. Huang, Y. Zhang, P. K. Liaw, and C. P. Chuang, Tensile deformation micromechanisms for bulk metallic glass matrix composites: From work-hardening to softening, Acta Mater. **59**, 4126 (2011).

[31] E. S. Park and D. H. Kim, Phase separation and enhancement of plasticity in Cu–Zr–Al–Y bulk metallic glasses, Acta Mater. **54**, 2597 (2006).

[32] B. J. Park, H. J. Chang, D. H. Kim, W. T. Kim, K. Chattopadhyay, T. A. Abinandanan, and S. Bhattacharyya, Phase Separating Bulk Metallic Glass: A Hierarchical Composite, Phys. Rev. Lett. **96**, 245503 (2006).